American Mineralogist, Volume 86, pages 1483–1488, 2001

Crystal structure of phase X, a high pressure alkali-rich hydrous silicate and its anhydrous equivalent

HEXIONG YANG,* JÜRGEN KONZETT,† AND CHARLES T. PREWITT

Geophysical Laboratory and Center for High Pressure Research, Carnegie Institution of Washington, 5251 Broad Branch Road N.W., Washington, D.C. 20015-1305, U.S.A.

ABSTRACT

Phase X, ascribed by Luth (1995) to a hydrous K-rich silicate formed from the breakdown of K-amphibole at high pressures, was synthesized at 1250–1300 °C and 10–16 GPa in four different compositions: $Na_{1.78}(Mg_{1.89}Al_{0.13})Si_{2.02}O_7$ (anhydrous sodic phase X), $Na_{1.16}K_{0.01}(Mg_{1.89}Al_{0.14})Si_{2.02}O_7H_{0.65}$ (sodic phase X), $K_{1.85}Mg_{2.06}Si_{2.01}O_7$ (anhydrous phase X), and $K_{1.54}Mg_{1.93}Si_{1.89}O_7H_{1.04}$ (phase X). A general chemical formula for these phases can be expressed as $A_{2-x}M_2Si_2O_7H_x$, with A = K and/or Na, M = Mg and/or Al, and x = 0–1. Structure determination from single-crystal X-ray diffraction data shows that anhydrous sodic phase X is trigonal with space group $P\bar{3}1m$, whereas the other three have an identical structure with space group $P6_3cm$. Both $P\bar{3}1m$ and $P6_3cm$ structures are characterized by MgO_6 octahedral layers that are stacked along the **c** axis and inter-linked together by Si_2O_7 tetrahedral dimers and K or Na cations. Within the MgO_6 layers, each MgO_6 octahedron shares three edges with neighboring MgO_6 octahedra to form brucite-like layers with one out of three octahedral sites vacant. Large K or Na cations are situated right below and above each occupied octahedron in the MgO_6 layers, whereas the Si_2O_7 groups are located below and above each vacant octahedron in the layers. The two types of structures, however, differ in the relative orientation of MgO_6 octahedral layers, the coordination of K or Na, and the configuration of SiO_4 tetrahedral dimers. By comparison, the $Na_2Mg_2Si_2O_7$ phase synthesized by Gasparik and Litvin (1997) appears to have the stoichiometry identical to anhydrous sodic phase X. Hence, these two high-pressure phases are likely to possess the same structure, or at least are closely related to each other structurally.

INTRODUCTION

A knowledge of the mechanisms by which potassium is stored and transported in the Earth's upper mantle and transition zone is of crucial importance to an understanding of alkali-rich magma generation in subduction zones and plume-related intra-plate settings. In portions of the peridotitic mantle accessible through xenoliths, the major carriers of potassium are hydrous potassic phases. Although clinopyroxene can accommodate K_2O on a wt% level under upper mantle pressures and temperatures (e.g., Harlow and Veblen 1991, Harlow 1997), the stability of a hydrous potassic phase or a hydrous melt precludes significant K partitioning into coexisting clinopyroxene (Luth 1997). The most common hydrous phases that can carry significant amounts of potassium in peridotitic mantle are phlogopite and calcic amphibole. The latter is restricted to low pressures in the range 2.2–3.0 GPa (Schmidt and Poli 1998 and references therein) and usually shows K_2O concentrations between 0.5 and 2.5 wt% (e.g., Wilkinson and LeMaitre 1987; Deer et al. 1997). Phlogopite, on the other hand, is stable to approximately 6.0 GPa in the presence of orthopyroxene and breaks down toward higher pressures to form potassium-amphibole (Konzett and Ulmer 1999). In the absence of orthopyroxene or in case the modal amount of phlogopite exceeds that of orthopyroxene, phlogopite may persist to pressures as high as 11–12 GPa before reacting to potassium-amphibole (Luth 1997). Potassium-amphibole stability is limited to approximately 14 GPa or 420 km depth in both natural (KLB-1, Takahashi 1986) and simplified bulk compositions (Inoue et al. 1998, Konzett and Fei 2000). At higher pressures potassium-amphibole breaks down to produce a hydrous potassium-rich silicate (Trønnes 1990; Luth 1995; Inoue et al. 1995), which was named phase X by Luth (1995). According to Luth (1997), phase X is stable to at least 1600 °C at 17 GPa in the system diopside + phlogopite. In a simplified K_2O-Na_2O-CaO-MgO-

* Present address: Jet Propulsion Laboratory, Mail Stop 183-301, 4800 Oak Grove Drive, Pasadena, CA 91109-8099, U.S.A. E-mail: yang@mail2.jpl.nasa.gov

† Present address: Institut für Mineralogie und Petrographie, Universität Innsbruck, Innrain 52, A-6020 Innsbruck, Austria.

Al_2O_3-SiO_2-H_2O system, phase X was found to be stable to 20 GPa and 1700 °C (Konzett and Fei 2000). This high thermal stability makes phase X a potential host for K, Na, and H_2O in metasomatized upper mantle and transition zone settings. In addition, phase X would also be a suitable host for trace elements with large ionic radii such as Rb, Cs, or Ba.

Inoue et al. (1998) proposed a formula $K_4Mg_8Si_8O_{25}(OH)_2$ with 1.7 ± 0.1 wt% H_2O for phase X, based on SIMS and microprobe analyses in the K_2O-CaO-MgO-SiO_2-H_2O system. Preliminary results by Konzett and Yang (1999), however, indicated a general formula $K_{2-x}Mg_2Si_2O_7H_x$ with x = 0–1, based on experiments in the K_2O-MgO-SiO_2-H_2O system. A variable stoichiometry of phase X would be consistent with results by Luth (1997) and Inoue et al. (1998) who reported variable K_2O contents (10.2–19.4 wt%) and analytical totals (91.5–98.2 wt%) of phase X, with a constant molar Mg/Si or (Mg + Al)/Si ratio of 1:1. The present study was undertaken to determine the crystal structure of phase X in simplified bulk compositions using single crystal X-ray analysis and to reconcile the results with the compositional variability of phase X.

Experimental and analytical techniques

The starting materials used for the synthesis experiments were made from high (≥99.99%) purity SiO_2, Al_2O_3, MgO, Na_2CO_3, and K_2CO_3 and assay-grade $Mg(OH)_2$. Oxides were fired at 1100 °C and carbonates/brucite dried at 250 °C overnight and immediately mixed in appropriate proportions. The mixtures were then decarbonated by step-heating to 900 °C with intermittent checks of loss on ignition. After decarbonation, water was added as brucite for water-bearing mixes. The starting materials were filled into 1.55 mm outer diameter Pt_{100} capsules, crimped and stored again at 250 °C overnight to minimize adsorption of moisture before welding shut.

For the present study, we report structural results from four synthesis experiments, namely JKW28, JKW42, JKW56, and JKW62 (Table 1). These experiments were conducted with a Walker-type multi-anvil apparatus at the Geophysical Laboratory using 10/5 (10 mm edge length of octahedra/5 mm truncated edge length of WC-cubes) MgO-octahedra/pyrophyllite gasket assemblies and an Re heater. Temperatures were measured using W3%Re-W25%Re thermocouples without correction for the pressure effect on electromotive force (emf). Both pressure and temperature were computer-controlled during the entire duration of the runs (7 to 24 hours) and kept constant to ±1 bar oil pressure in the hydraulic system and ± 3 °C. A detailed description of the experimental setup and calibration procedure is given by Bertka and Fei (1997). After the experiment the Pt capsule was embedded in epoxy resin and ground to expose the experimental charge for optical and microprobe examination. Because the alkali-rich phases were found to be very sensitive to beam damage and loss of alkalis, electron microprobe (JEOL superprobe) analytical conditions of 15 kV and 5 nA were used with a rastered electron beam of 20 μm size. Counting times were 20 s on peaks and 10 on backgrounds of the relevant X-ray lines without peak search on the unknowns to minimize the residence time of the electron beam. The following standards were used Si:SiO_2; Al:Al_2O_3; Mg:MgO; Ca:natural wollastonite; Na:synthetic omphacite; K:natural orthoclase and NIST standard glass K1597. The use of different standard combinations and slight variations in the thickness of the carbon-coating resulted in relative variations of the microprobe analyses within 1.0 to 1.5 wt% for Si, Mg, Na, and K.

Raman spectra were recorded with a Dilor XY confocal microRaman spectrometer equipped with a cryogenic Wright Model CCD detector. The excitation source was the 514 nm line of a coherent Innova Model 90-5 Ar^+ laser operating at 150 mW.

A single-crystal fragment was extracted from each charge for the structure study based on optical examination, precession photography, and X-ray diffraction peak profiles. X-ray precession photographs showed that the JKW42 crystal possesses trigonal symmetry, whereas the other three probably have the same hexagonal symmetry. All four crystals displayed streaks on their 00*l* reflections, indicating some structural defects or disorder along the **c** axis. Detailed X-ray experimental procedures were similar to those described by Yang et al. (1999). The unit-cell parameters of four samples are listed in Table 1.

Digitized ω step-scan data also showed the significant broadening of peak profiles of the 00*l* reflections for all crystals. Examination of measured reflections suggested the possible space groups $P312$, $P31m$, or $P\bar{3}1m$ for JKW42 and $P6_3cm$, $P\bar{6}c2$, or $P6_3/mcm$ for JKW28, JKW56, and JKW62. The *E*-value statistics of reflection data suggested a centric structure for JKW42 and a non-centric structure for JKW28, JKW56, or JKW62. For this reason, we first solved and refined the JKW42 structure with space group $P\bar{3}1m$ and the JKW56 structure with space group $P6_3cm$ using SHELX97. We also attempted the structure solution based on space group $P\bar{6}c2$ for JKW56, but were unable to obtain a reasonable structural model. The structures of JKW28 and JKW62 were found to be identical to that of JKW56. Difference-Fourier maps at convergence of the anisotropic refinements, however, failed to locate the H positions in any sample, perhaps because of the relatively poor quality of crystals along their **c** directions. The occupancies of the K/Na and Mg/Al cations at the A and M sites, respectively, were constrained to the chemical composition obtained from the electron microprobe analyses. The resulting formulas of

Table 1. Crystal data of phase X synthesized at high temperatures and pressures

Exp. no.	*a* (Å)	*c* (Å)	*V* (Å^3)	S.G.	d(g/cm^3)	Composition	Synthesis condition	Refl. > 2σ(*I*)	*R*-factor
JKW42	4.9827(4)	6.4354(10)	138.37(3)	$P\bar{3}1m$	3.10	$Na_{1.78}(Mg_{1.89}Al_{0.13})Si_{2.02}O_7$	10 GPa, 1250 °C	161	0.053
JKW28	4.976(1)	12.896(2)	276.5(1)	$P6_3cm$	2.95	$Na_{1.16}K_{0.01}(Mg_{1.89}Al_{0.14})Si_{2.02}O7H_{0.65}$	10 GPa, 1300 °C	246	0.046
JKW62	5.0685(3)	13.2226(4)	294.18(4)	$P6_3cm$	3.28	$K_{1.85}Mg_{2.06}Si_{2.01}O_7$	16 GPa, 1300 °C	233	0.042
JKW56	5.0812(4)	13.2112(9)	295.40(5)	$P6_3cm$	3.07	$K_{1.54}Mg_{1.93}Si_{1.89}O_7H_{1.04}$	16 GPa, 1300 °C	289	0.037

Note: $R = \Sigma||F_o| - |F_c|| / \Sigma |F_o|$.

four samples are given in Table 1. Because of the structural similarity of JKW28, JKW56, and JKW62, we report atomic positional coordinates and selected bond distances for JKW42 and JKW56 only (Tables 2 and 3).

RESULTS AND DISCUSSION

Nomenclature of the phases studied

To be consistent with the literature (Inoue et al. 1995; Luth 1995, 1997) and to facilitate reference to the phases examined in this study we have adopted the following terms based on the structure analysis and Raman spectroscopy: (K,Na)-Mg-silicates with Raman peaks in the OH-stretching region will be referred to as phase X or sodic phase X when Na is the dominant alkali element. Likewise, (K,Na)-Mg silicates lacking peaks in the OH-stretching region but otherwise similar Raman spectra will be referred to as anhydrous phase X or anhydrous sodic phase X.

Structures of phase X (JKW56)

The crystal structure of phase X is characterized by MgO_6 octahedral layers that are stacked along the **c** axis and interlinked by Si_2O_7 tetrahedral dimers and K cations (Figs. 1a and 1b). In the MgO_6 octahedral layers, each MgO_6 octahedron shares three edges with others to form brucite-like layers with one of three octahedral sites vacant. A similar layer configuration has been observed in the structure of phase D (Yang et al. 1997). Whereas K cations are situated below and above each occupied octahedron in the MgO_6 octahedral layers, the Si_2O_7 tetrahedral dimers are located below and above each vacant octahedron. Each K cation is coordinated by nine O atoms with an average bond distance of 2.803 Å. The nearest six O atoms form a trigonal prism around K and the next-nearest three O atoms are also bonded to two Si atoms each. In the Si_2O_7 dimer, both tetrahedra are elongated along the **c** axis, with the Si2 tetrahedron appearing to be more distorted than the Si1 tetrahedron (Table 1). However, considering the relatively large experimental uncertainty for the *z* coordinate of the O1 atom, which is likely to be associated with structural imperfection along the **c** direction, the real geometrical difference between the two tetrahedra may be smaller than observed. Another high-pressure structure containing the Si_2O_7 group has been found for a sodium trisilicate with composition $Na_2Si(Si_2O_7)$ (Fleet and Henderson 1995).

The H positions in phase X could not be unambiguously located. In general, hydrogen atoms do not bond to O atoms that belong to an SiO_4 tetrahedron, except for some rare cases, such as in hydrogarnet where 4 H^+ provide charge balance in vacant Si tetrahedra (Lager et al. 1987, 1989). However, all three symmetrically nonequivalent O atoms in the phase X structure are directly bonded to Si to form Si_2O_7 dimers. Among them, O1 is the bridging atom connecting Si1 and Si2 atoms, and O2 and O3 are non-bridging atoms. Accordingly, we assume that the latter two are candidates for hydrogen bonding. As the Raman spectrum of phase X (Fig. 2) exhibits two peaks in the O-H stretching region, indicating the existence of two possible OH positions, we, therefore, propose that the two non-bridging O atoms O2 and O3 are most likely bonded to H. Yet, two other related issues remain to be answered. The first one is the mechanism involved in hydrogen bonding and the second is whether or not the H atoms are ordered in the structure. For phase X (JKW56), there is a slight deficiency of Si based on the microprobe analysis (Table 1), which might indicate a bonding mechanism similar to that in hydrous garnet. However, such a deficiency can also be an artifact as the result of beam damage and/or loss of alkalis during microprobe analysis. Hydrogarnet-like hydrogen bonding cannot be invoked for sodic phase X (JKW28) because it shows nearly perfectly stoichiometric Si. Also, based on the available data, we cannot rule out the possibility of a coupled substitution involving H located in

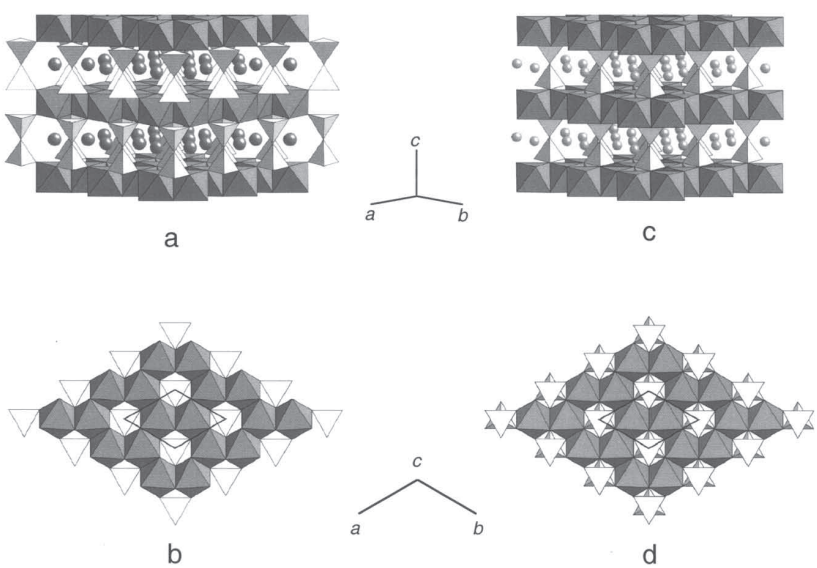

FIGURE 1. Crystal structures of phase X (**a** and **b**) with space group $P6_3cm$ and anhydrous sodic phase X (**c** and **d**) with space group $P\bar{3}1m$. For comparison, the *c* dimension of anhydrous sodic phase X is doubled (**a**).

the region of a K vacancy and bonded to the bridging O atom where one of the Si sites is vacant. Evidently, the complete structure of phase X remains a mystery until these questions can be addressed.

Structure of anhydrous sodic phase X (JKW42)

Although the space group of JKW42 differs from that of JKW56, their structures are comparable in many aspects. Like phase X, the structure of JKW42 consists of MgO_6 octahedral layers stacked in the **c** direction and interconnected by Si_2O_7 tetrahedral dimers and Na cations (Figs. 1c and 1d). The respective locations of the Si_2O_7 dimers and Na cations relative to the MgO_6 octahedral layers in anhydrous sodic phase X are also similar to the tetrahedral dimers and K cations in phase X. However, there are three major differences between the two structures: (1) There are two MgO_6 octahedral layers in the unit cell of phase X with two successive layers having + – orientation (Fig. 1a), but only one MgO_6 octahedral layer in the unit cell of the anhydrous sodic phase X with two successive layers having + + orientation; (2) in contrast to phase X where the six nearest O atoms form a trigonal prism around K or Na, the six nearest O atoms in anhydrous sodic phase X form a trigonal antiprism around Na; (3) the two SiO_4 tetrahedra that form a dimer in phase X seem to be related to each other by a pseudo mirror plane (Fig. 1a), whereas the two SiO_4 tetrahedra in a dimer in anhydrous sodic phase X are related to each other by a center of inversion (Fig. 1c) and they are slightly compressed along the **c** axis. Owing to the size difference between K and Na, the separation of the two MgO_6 layers in JKW42 (6.435 Å) is significantly smaller than that (6.606 Å) in JKW56. The large separation in phase X is principally achieved by elongation of the SiO_4 tetrahedra along the **c** axis and an increased distance between Si cations (3.375 Å in phase X vs. 3.244 Å in anhydrous sodic phase X).

The structural relationship between phase X and anhydrous sodic phase X can also be viewed in another way. If we regard an MgO_6 octahedral layer and those tetrahedra that are just below and above the layer as a composite layer (Fig. 3a), then the structure of anhydrous sodic phase X is simply a result of stacking of such composite layers along the **c** direction (Fig. 3c). The phase X structure, then, can be readily obtained by rotating every other layer in anhydrous sodic phase X by ±60° or ±180° around the **c** axis (Fig. 3b). Although it is still not clear to us why anhydrous sodic phase X possesses the $P\bar{3}1m$ structure whereas the three examined samples have the $P6_3cm$ structure, the close relationship between the two types of the structures would suggest similar energetics of formation. Therefore, it follows that it

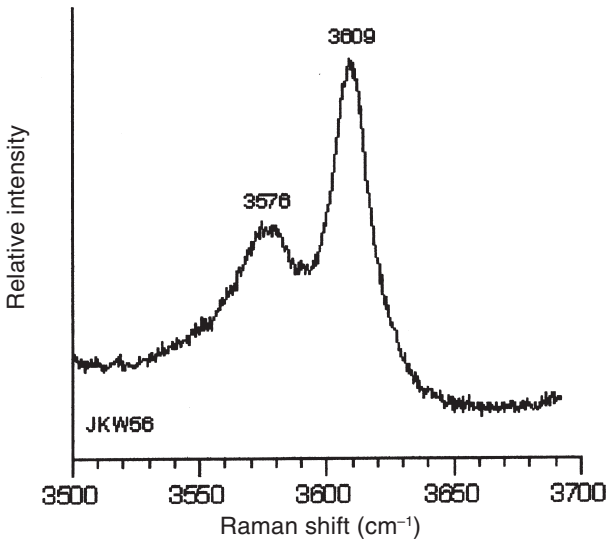

FIGURE 2. Raman spectrum of phase X ($K_{1.54}Mg_{1.93}Si_{1.89}O_7H_{1.04}$) (JKW56).

TABLE 2. Atomic coordinates and isotropic displacement factors of phase X

Site		JKW42	Site		JKW56
A	x	1/3	A	x	1/3
	y	2/3		y	2/3
	z	1/2		z	0.2072(4)
	U_{eq}	0.042(2)		U_{eq}	0.017(1)
M	x	2/3	M	x	1/3
	y	1/3		y	2/3
	z	0		z	0.4541(4)
	U_{eq}	0.011(1)		U_{eq}	0.008(1)
Si	x	0	Si1	x	0
	y	0		y	0
	z	0.2480(2)		z	0.0792(3)
	U_{eq}	0.009(1)		U_{eq}	0.002(1)
			Si2	x	0
				y	0
				z	0.3347(3)
				U_{eq}	0.008(1)
O1	x	0	O1	x	0
	y	0		y	0
	z	1/2		z	0.2056(12)
	U_{eq}	0.054(5)		U_{eq}	0.010(1)
O2	x	0.3187(6)	O2	x	0.3102(5)
	y	0		y	0
	z	0.8156(5)		z	0.0458(9)
	U_{eq}	0.015(2)		U_{eq}	0.009(2)
			O3	x	0.3081(7)
				y	0
				z	0.3634(9)
				U_{eq}	0.006(2)

Note: $U_{eq} = (1/3)\Sigma_i\Sigma_j U_{ij} a_i^* a_j^* a_i a_j$.

TABLE 3. Selected interatomic bond distances of phase X

$P\bar{3}1m$	JKW42	$P6_3cm$	JKW56
A-O1 (×3)	2.877(1)	A-O1 (×3)	2.934(1)
A-O2 (×6)	2.648(3)	A-O2 (×3)	2.761(8)
Avg.	2.724	A-O3 (×3)	2.714(8)
		Avg.	2.803
M-O2 (×6)	2.072(3)	M-O2 (×3)	2.133(9)
Avg.	2.072	M-O3 (×3)	2.130(9)
		Avg.	2.132
Si1-O1	1.622(2)	Si1-O1	1.669(18)
Si1-O2 (×3)	1.640(4)	Si1-O2 (×3)	1.637(5)
Avg.	1.636	Avg.	1.645
		Si2-O1	1.706(17)
		Si2-O3 (×3)	1.611(5)
		Avg.	1.635

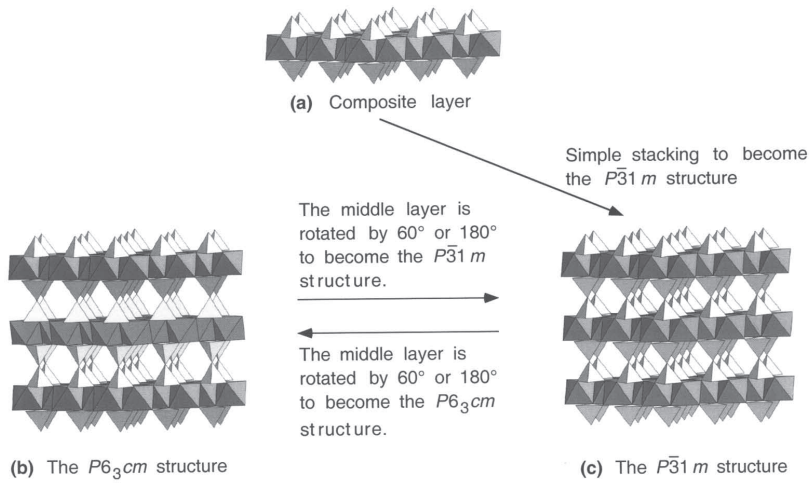

FIGURE 3. (**a**) A composite layer. It consists of an MgO_6 octahedral layer and those tetrahedra that are directly bonded to and right below and above the layer. (**b**) The phase X structure can be readily obtained by rotating every other layer in the hydrous potassic phase X by 60° or 180° around the **c** axis, or vice versa. For simplicity, large cations K and Na are left out in the figure. (**c**) The structure of anhydrous sodic phase X can be regarded as a result of simple stacking of such composite layers along the **c** direction.

should not be unusual to form stacking disorder of the composite layers along the **c** axis in either phase, giving us a plausible explanation for the observed broadening of the 00*l* reflections parallel to **c** for all the samples studied in this work.

It is interesting to note that Gasparik and Litvin (1997) performed a series of high-pressure melting experiments on the join Mg_2SiO_4-$NaAlSi_2O_6$ between 4 and 22 GPa and found that, below the solidus, forsterite-rich compositions produced a divariant assemblage of forsterite, clinopyroxene, garnet, and an unknown phase with composition $Na_2Mg_2Si_2O_7$. They further suggested that the $Na_2Mg_2Si_2O_7$ phase may be present in the Earth's mantle in nepheline-normative compositions due to the instability of nepheline at higher pressures. Unfortunately, no crystallographic data were given for the new high-pressure phase. By comparison with the results reported here, it is apparent that the $Na_2Mg_2Si_2O_7$ phase synthesized by Gasparik and Litvin (1997) is identical to anhydrous sodic phase X. Hence, it can be assumed that the two high-pressure phases are likely to possess the same structure, or at least are closely related to each other structurally.

CONCLUSIONS

Several high-pressure anhydrous and hydrous phases that contain large alkali cations have recently been synthesized and characterized structurally, such as $Na_2Si(Si_2O_7)$ (Fleet and Henderson 1995), $Na_{1.8}Ca_{1.1}Si_6O_{14}$ (Gasparik et al. 1995), $Na_6Si_3(Si_9O_{27})$ (Fleet 1996), $Na_2Mg_{4+x}Fe^{3+}_{2-2x}Si_{6+x}O_{20}$ (Gasparik et al. 1999), $K(KCa)Mg_5Si_8O_{22}(OH)_2$ (Yang et al. 1999), $Na_2Mg_6Si_6O_{18}(OH)_2$ (Yang and Konzett 2000), $K_{1.10}Na_{2.32}Ca_{1.52}Mg_{5.85}Al_{1.23}Si_{12.04}O_{34}(OH)_2$ (Yang et al. 2001), as well as phase X and anhydrous phase X (this study). One the one hand, these new structure data not only have enriched our knowledge of crystal chemistry in general, but also extended our understanding of the high-pressure behavior of alkali-bearing structures in particular. On the other, they have presented themselves as new challenges to us, like the problems related to H in phase X. Therefore, more systematic investigations combining structure refinements with other state-of-art spectroscopic techniques are necessary for us to gain a better understanding of crystal chemistry of high-pressure phases.

ACKNOWLEDGMENTS

This work was supported by NSF grant EAR-9973018 and the Center for High Pressure Research. After the manuscript for this paper was submitted, we received a preprint from F. Mancini, G. Harlow, and C. Cahill, who described a similar study of the hydrous K phase X and also submitted it to the journal. We note that their results are complementary to ours.

REFERENCES CITED

Bertka, C.M. and Fei, Y. (1997) Mineralogy of the Martian interior up to core-mantle boundary pressures. Journal of Geophysical Research, 102, 5251–5264.

Deer, W.A., Howie, R.A., and Zussman, J. (1997) Calcic amphiboles—Hornblende group. In Deer, W.A., Howie, R.A. and Zussman, J., Rock-forming minerals, vol. 2B (2nd ed.) Double chain silicates, p. 233–613. The Geological Society of London, U.K.

Fleet, M.E. (1996) Sodium tetrasilicate: A complex high-pressure framework silicate ($Na_6Si_3[Si_9O_{27}]$). American Mineralogist, 81, 1105–1110.

Fleet, M.E. and Henderson, G.S. (1995) Sodium trisilicate: A new high-pressure silicate structure ($Na_2Si[Si_2O_7]$). Physics and Chemistry of Minerals, 22, 383–386.

Gasparik, T. and Litvin, Y.A. (1997) Stability of $Na_2Mg_2Si_2O_7$ and melting relations on the forsterite-jadeite join at pressures up to 22 GPa. European Journal of Mineralogy, 9, 311–326.

Gasparik, T, Parise, J.B., Eiben, B.A., and Hriljac, J.A. (1995) Stability and structure of a new high-pressure silicate, $Na_{1.8}Ca_{1.1}Si_6O_{14}$. American Mineralogist, 80, 1269–1276.

Gasparik, T., Parise, J.B., Reeder, R.J., Young, V.G., and Wilford, W.S. (1999) Composition, stability, and structure of a new member of the aenigmatite group, $Na_2Mg_{4+x}Fe^{3+}_{2-2x}Si_{6+x}O_{20}$, synthesized at 13–14 GPa. American Mineralogist, 84, 257–266.

Harlow, G.E. (1997) K in clinopyroxene at high pressure and temperature: an experimental study. American Mineralogist, 82, 259–269.

Harlow, G.E. and Veblen, D.R. (1991) Potassium in clinopyroxene: inclusions from diamonds. Science, 251, 652–655.

Inoue, T., Irifune, T., Yorimoto, H., and Miyagi, I. (1995) Decomposition of K-amphibole at high pressure: implications for the origin of the third chain volcanism. EOS, Transactions, American Geophysical Union, 76, F711.

Inoue, T., Irifune, T., Yurimoto, H., and Miyagi, I. (1998) Decomposition of K-amphibole at high pressures and implications for subduction zone volcanism. Physics of the Earth and Planetary Interiors, 107, 221–231.

Konzett, J. and Fei, Y. (2000) Transport and storage of potassium in the Earth's upper mantle and transition zone: an experimental study to 23 GPa in simplified and natural bulk compositions. Journal of Petrology, 41, 583–603.

Konzett, J. and Ulmer, P. (1999) The stability of hydrous potassic phases in lherzolitic mantle—an experimental study to 9.5 GPa in simplified and natural bulk compositions. Journal of Petrology, 40, 629–652.

Konzett, J. and Yang, H. (1999) Stability and structure of phase X—a high pressure hydrous potassium silicate. In Mysen, B., Rubie, D., Ulmer, P. and Walter, M. convenors, Processes and consequences of deep subduction, Terra Nostra, 99/7, p. 60–62. Alfred-Wegener-Stiftung, Bonn.

Lager, G.A., Armbruster, T., and Faber, F. (1987) Neutron and X-ray diffraction study of hydrogarnet $Ca_3Al_2(O_4H_4)_3$. American Mineralogist, 72, 756–765.

Lager, G.A., Armbruster, T., Rotella, F.J., and Rossman, G.R. (1989) OH substitution in garnets. X-ray and neutron diffration, infrared, and geometric modeling

studies. American Mineralogist, 74, 840–851.
Luth, R.W. (1995) Potassium in pyroxenes at high pressure. EOS, Transactions, American Geophysical Union, 76, F711.
———(1997) Experimental study of the system phlogopite-diopside from 3.5–17 GPa. American Mineralogist, 82, 1198–1209.
Schmidt, M.W. and Poli, S. (1998) Experimentally based water budgets for dehydrating slabs and consequences for arc magma generation. Earth and Planetary Science Letters, 163, 361–379.
Takahashi, E. (1986) Melting of dry peridotite KLB-1 up to 14 GPa: implications on the origin of peridotitic upper mantle. Journal of Geophysical Research, 91, 9367–9382.
Trønnes, R.G. (1990) Low-Al, high-K amphiboles in subducted lithosphere from 200 to 400 km depth: experimental evidence. EOS, Transactions, American Geophysical Union, 71, F1587.
Wilkinson, J.F.G. and LeMaitre, R.W. (1987) Upper mantle amphiboles and micas and TiO_2, K_2O, and P_2O_5 abundances and 100 Mg/(Mg+Fe^{2+}) ratios of common basalts and andesites: implications for modal mantle metasomatism and undepleted mantle compositions. Journal of Petrology, 28, 37–73.
Yang, H. and Konzett, J. (2000) High-pressure synthesis of $Na_2Mg_6Si_6O_{18}(OH)_2$—a new hydrous silicate phase isostructural with aenigmatite. American Mineralogist, 85, 259–262.
Yang, H., Prewitt, C.T., and Frost, D.J. (1997) Crystal structure of the dense hydrous magnesium silicate, phase D. American Mineralogist, 82, 651–654.
Yang, H., Konzett, J., Prewitt, C.T., and Fei, Y. (1999) Single-crystal structure refinement of synthetic ^{M4}K-substituted potassic richterite, $K(KCa)Mg_5Si_8O_{22}(OH)_2$. American Mineralogist, 84, 681–684.
Yang, H., Konzett, J., and Prewitt, C.T. (2001) Crystal structure of a new clinopyribole synthesized at high temperature and pressure. American Mineralogist, 86, 1261–1266.

MANUSCRIPT RECEIVED JANUARY 19, 2001
MANUSCRIPT ACCEPTED JULY 17, 2001
MANUSCRIPT HANDLED BY JAMES W. DOWNS